Talanta 218 (2020) 121101

Contents lists available at ScienceDirect

Talanta

journal homepage: www.elsevier.com/locate/talanta

Persistent luminescence nanorod based luminescence resonance energy transfer aptasensor for autofluorescence-free detection of mycotoxin

Yuan-Yuan Jiang[a,b,c], Xu Zhao[a,b,c], Li-Jian Chen[a,b,c], Cheng Yang[a,b,c], Xue-Bo Yin[d], Xiu-Ping Yan[a,b,c,*]

[a] State Key Laboratory of Food Science and Technology, Jiangnan University, Wuxi, 214122, China
[b] International Joint Laboratory on Food Safety, Jiangnan University, Wuxi, 214122, China
[c] Institute of Analytical Food Safety, School of Food Science and Technology, Jiangnan University, Wuxi, 214122, China
[d] Research Center for Analytical Science, College of Chemistry, Nankai University, Tianjin, 300071, China

ARTICLE INFO

Keywords:
Ochratoxin A
Beer
Aptasensor
Persistent luminescence
Autofluorescence-free detection

ABSTRACT

Serious ochratoxin A (OTA) contamination necessitates the development of rapid, sensitive and selective analytical methods for its determination in food safety. Herein, we report a persistent luminescence resonance energy transfer (LRET) based aptasensor for the autofluorescence-free detection of OTA. OTA aptamer functionalized persistent luminescence nanorod (PLNR) Zn_2GeO_4:Mn^{2+} and the aptamer complementary DNA modified gold nanoparticle (AuNP) were used as the donor and the acceptor, respectively. The developed LRET aptasensor integrated the advantages of the long-lasting persistent luminescence of PLNR, the high selectivity of aptamer and the low probe background of LRET sensors, allowing autofluorescence-free detection of OTA in biological samples with high sensitivity and selectivity. The developed LRET aptasensor gave an excellent linearity in the range of 0.01–10 ng mL^{-1}, the detection limit of 3 pg mL^{-1} and the precision of 2.7% (RSD, n = 11) at 1 ng mL^{-1} level. The applicability of the developed aptasensor was demonstrated by analyzing beer samples for OTA with the recoveries of 92.3%–104%.

1. Introduction

Ochratoxin A (OTA), a foodborne mycotoxin mainly produced by *Aspergillus* and *Penicillium*, exists in various food matrices, such as cereals, coffee, dried fruits, wine, grape juice and beer [1–4]. OTA could cause hepatotoxic, carcinogenic, nephrotoxic and immunotoxic effects on humans, so OTA contamination is a critical food safety issue [5,6]. Many countries have set regulatory limits on the level of OTA in foodstuffs. For instance, European Commission has established the maximum acceptable level of OTA at 5 μg kg^{-1} for raw cereal grains, 10 μg kg^{-1} for dried fruits, 2 μg kg^{-1} for grape juice and wine [7,8].

Several analytical techniques have been developed for the detection of OTA, including high-performance liquid chromatography, mass spectrometry, gas chromatography, electrochemical method and enzyme-linked immunosorbent assay (ELISA) [9–15]. Fluorescence spectrometry is increasingly used for biodetection due to its simplicity and high sensitivity. Quite a few of fluorescent probes including organic dyes, quantum dots and upconversion nanoparticles have been successfully developed for the detection of OTA [16–19]. However, conventional fluorescence methods may suffer from autofluorescence interferences. Thus, a simple, highly selective and sensitive method for autofluorescence-free detection of OTA in real samples is desirable.

Persistent luminescence nanoparticles can store excitation energy and emit long-lasting luminescence slowly after excitation ceases [20–23]. Such luminescent feature allows optical detection without external illumination to avoid scattering light and autofluorescence interferences from complex matrixes and achieve high signal-to-noise ratio [24–26]. So far, a number of persistent luminescence nanoparticles based probes have been successfully applied in biosensing [27–29], bioimaging [30–34] and imaging-guided cancer therapy [35–37]. However, to the best of our knowledge, persistent luminescence nanomaterials based methods for autofluorescence-free determination of OTA have not been reported so far.

Herein, we report a persistent luminescence aptasensor for autofluorescence-free detection of OTA based on luminescence resonance energy transfer (LRET). OTA aptamer functionalized persistent luminescence nanorod (PLNR) Zn_2GeO_4:Mn^{2+} was used as the donor and aptamer complementary DNA (cDNA) modified gold nanoparticle (AuNP) as the acceptor. The developed aptasensor integrates the advantages of autofluorescence-free persistent luminescence detection,

* Corresponding author. State Key Laboratory of Food Science and Technology, Jiangnan University, Wuxi, 214122, China.
E-mail address: xpyan@jiangnan.edu.cn (X.-P. Yan).

https://doi.org/10.1016/j.talanta.2020.121101
Received 27 March 2020; Received in revised form 21 April 2020; Accepted 27 April 2020
Available online 01 May 2020
0039-9140/

high selectivity of aptamer and LRET based low probe background, allowing sensitive and selective detection of OTA in real samples.

2. Experimental

2.1. Materials and reagents

Zinc nitrate hexahydrate ($Zn(NO_3)_2{\cdot}6H_2O$), manganese nitrate ($Mn(NO_3)_2$), germanium oxide (GeO_2), chloroauric acid ($HAuCl_4{\cdot}4H_2O$), (3-aminopropyl)triethoxysilane (APTES), 4-(*N*-maleimidomethyl)cyclohexane-1-carboxylic acid 3-sulfo-*N*-hydroxysuccinimide ester sodium salt (Sulfo-SMCC), sodium dodecyl sulfate (SDS), 4-(2-hydroxyethyl)-1-piperazineethanesulfonic acid (HEPES) and tris(hydroxymethyl)aminomethane hydrochloride (Tris-HCl) were purchased from Aladdin (Shanghai, China). *N*,*N*-dimethylformamide (DMF), sodium hydroxide (NaOH), ammonium hydroxide ($NH_3{\cdot}H_2O$), sodium chloride (NaCl), sodium bicarbonate ($NaHCO_3$), trisodium citrate and concentrated nitric acid (HNO_3) were purchased from Sinopharm Chemical Reagent Co., Ltd. (Shanghai, China). OTA, aflatoxin B1 (AFB1), and zearalenone (ZEN) were purchased from Sigma-Aldrich (St. Louis, MO). Ochratoxin B (OTB), fumonisin (FB1) and deoxynivalenol (DON) were purchased from Beijing ShiJiAoKe Biotech Co., Ltd. (Beijing, China). The OTA ELISA Kit was purchased from Shanghai YouLong Biotech Co., Ltd. (Shanghai, China). The sequence of OTA aptamer and the complementary DNA (SH-cDNA) of OTA aptamer (Sangon Biotechnology Co., Ltd., Shanghai, China) are shown in Table S1. All chemicals used are at least analytical grade and used without further purification.

2.2. Instrumentation

Transmission electron microscopic (TEM) images were obtained on a JEM-2100 transmission electron microscope (200 kV, JEOL, Japan). X-ray diffraction (XRD) patterns were recorded on a D2 PHASER powder diffractometer with a CuKα radiation source (Bruker, Germany). UV–vis absorption spectra were measured on a UV-3600PLUS UV–vis–NIR spectrophotometer (Shimadzu, Japan). Persistent luminescence spectra were recorded on an F-7000 fluorescence spectrometer (Hitachi, Japan). Photoluminescence quantum yield was obtained on an FLS920 spectrometer (Edinburgh, UK). Dynamic light scattering (DLS) and zeta potential were measured on a Nano ZS Zetasizer (Malvern, UK). Fourier transform infrared (FT-IR) spectra were acquired on an IS10 FTIR spectrometer (Nicolet, USA).

2.3. Synthesis and functionalization of PLNR

$Zn_2GeO_4{:}Mn^{2+}$ PLNR was synthesized according to a hydrothermal procedure [38,39]. GeO_2 was dissolved in NaOH solution (2 mol L^{-1}) to obtain Na_2GeO_3 solution (1 mol L^{-1}). $Mn(NO_3)_2$ (0.005 mmol) and $Zn(NO_3)_2$ (2 mmol) were dissolved in 10 mL ultrapure water, and mixed with 300 μL of HNO_3 (68%, wt) under vigorous stirring. Na_2GeO_3 (1 mmol) was then dropwise added to the above solution. The mixture was adjusted to pH 9.0 with $NH_3{\cdot}H_2O$ (28%, wt), kept stirring for 1 h at room temperature, transferred to a 30 mL Teflon-lined autoclave and kept at 220 °C for 6 h. The final products were washed several times with ultrapure water, and dried under vacuum. The obtained PLNR powder was dispersed in 5 mmol L^{-1} NaOH solution under ultrasonic treatment for 1 h. After overnight stirring, the resultant colloidal solution was centrifuged and washed with ultrapure water, the resulting hydroxylated PLNR (PLNR-OH) were thus acquired after vacuum dry.

The amino-functionalized PLNR (PLNR-NH_2) was obtained according to our previous work [34]. Briefly, 100 mg of PLNR-OH was dispersed in 40 mL of DMF with sonication, then 400 μL of APTES was dropwise added under vigorous stirring. The reaction mixture was incubated at 80 °C for 12 h. The obtained PLNR-NH_2 was collected by centrifugation, washed with DMF and dried under vacuum.

2.4. Preparation of OTA aptamer modified PLNR (PLNR-Apt)

Briefly, 3 mg of PLNR-NH_2 was dispersed in 2.1 mL of HEPES buffer (10 mmol L^{-1}, pH 7.2) under sonication, then 0.9 mg of sulfo-SMCC in 900 μL of DMF was added. The mixture was incubated for 2 h with gentle shaking. The obtained maleimide-activated PLNR-NH_2 was centrifuged at 6000 rpm for 5 min, washed with phosphate buffer saline (PBS, 137 mmol L^{-1} NaCl, 2.7 mmol L^{-1} KCl, 8.7 mmol L^{-1} Na_2HPO_4 and 1.4 mmol L^{-1} KH_2PO_4, pH 7.4) three times, and redispersed in 3 mL of PBS buffer. Further functionalization of the OTA aptamer was performed by mixing 5.6 nmol of aptamer with maleimide-activated PLNR-NH_2 with shaking at room temperature for 12 h. The resultant nanoparticles were collected by centrifugation, and the excess aptamer was removed by washing with PBS buffer three times. The resulting PLNR-Apt was finally redispersed in 3 mL of Tris-HCl buffer (10 mmol L^{-1}, pH 8.0, containing 10 mmol L^{-1} NaCl) for further use.

2.5. Synthesis of cDNA modified AuNP (AuNP-cDNA)

AuNP was prepared according to previous publications [40,41]. 34 μL of SH-cDNA (10 μmol L^{-1}) was added to 5 mL of AuNP (3.4 nmol L^{-1}) solution, the mixture was then shaken for 12 h at room temperature. Phosphate buffer (0.1 mol L^{-1} NaH_2PO_4-Na_2HPO_4, pH 7.4) and SDS solution (10%) were added to the mixture to reach a concentration of 0.01 mol L^{-1} and 0.01%. Subsequently, NaCl solution (2.0 mol L^{-1}) was slowly added to the above solution within 6 h to obtain a final NaCl concentration of 0.01 mol L^{-1}. The final product was centrifuged at 10 000 rpm for 15 min, washed with Tris-HCl three times, then resuspended in Tris-HCl buffer for further use.

2.6. Preparation of beer samples

Beer samples were collected from local supermarkets. 20 mL of the degassed beer sample was transferred into a 25 mL volumetric flask, the aqueous solution containing 15% NaCl and 2% $NaHCO_3$ was then added to volume and thoroughly mixed. The resulting solution was filtered and the filtrate was collected for the determination of OTA by the developed method. For the recovery experiments, the beer samples were spiked with various amounts of OTA before sample preparation.

2.7. Procedure for determination of OTA

260 μL of PLNR-Apt (1 mg mL^{-1}), 123 μL of AuNP-cDNA (1.7 nmol L^{-1}) and 1.35 mL of Tris-HCl buffer were added into a 2 mL calibrated test tube, the mixture was incubated for 120 min at room temperature. Subsequently, a given concentration of OTA standard solution or the beer sample solution was added. The solution was then diluted to volume with ultrapure water and further incubated for 60 min. Finally, the persistent luminescence (PL) intensity was measured using a fluorescence spectrometer in phosphorescence mode with an excitation wavelength of 254 nm. The slit widths for excitation and emission were both set at 5 nm.

3. Results and discussion

3.1. Design and principle of the LRET aptasensor

Fig. 1 shows the scheme for the development of the PLNR based LRET aptasensor for autofluorescence-free detection of OTA. To overcome the problem with the autofluorescence interference encountered in conventional fluorescence detection, PLNR $Zn_2GeO_4{:}Mn^{2+}$ was used as the luminescence source due to the long lasting persistent luminescence property [21]. The long lasting persistent luminescence permits the detection of luminescence without the need for external excitation, thereby eliminating interference associated with background autofluorescence and light scattering from matrixes. To achieve high

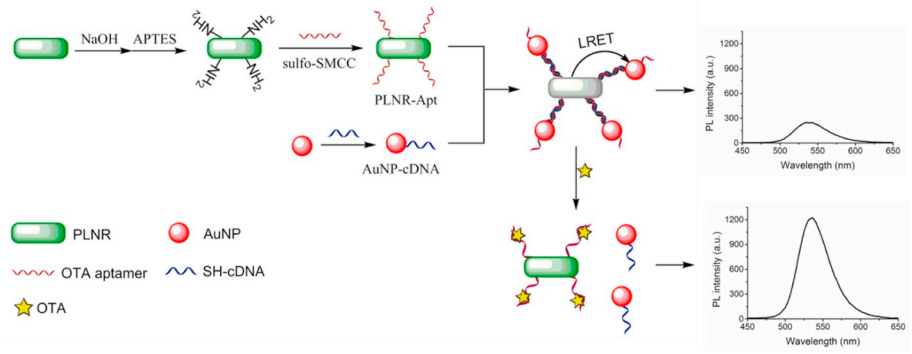

Fig. 1. Schematic illustration of the PLNR based LRET aptasensor for the detection of OTA.

selectivity and sensitivity for OTA detection, OTA aptamer conjugated PLNR (PLNR-Apt) was used as the energy donor, while AuNP modified with partially complementary DNA (AuNP-cDNA) was used as the energy acceptor because of the easy surface modification and the large overlap between the absorption spectra of AuNP and the persistent luminescence emission spectra of PLNR. In the absence of OTA, PLNR-Apt was hybridized with AuNP-cDNA between the complimentary oligonucleotide pairs, leading to significant luminescence quenching of PLNR due to the energy transfer from PLNR-Apt to AuNP-cDNA. In the presence of OTA, the aptamer preferentially bound with OTA to detach AuNP-cDNA from PLNR-Apt, recovering persistent luminescence for OTA detection.

3.2. Preparation, surface modification and characterization of PLNR and AuNP

The PLNR Zn_2GeO_4:Mn^{2+} was synthesized using a direct hydrothermal method [38,39]. The as-prepared PLNR displayed high crystallinity with a standard rhombohedral phase of Zn_2GeO_4 (JCPDS 11-0687) (Fig. 2A), and exhibited good dispersity and typical rod shape with the mean length and width of *ca.* 65 nm and 20 nm, respectively (Fig. 2B). The as-prepared PLNR emitted bright green luminescence at 536 nm due to the $^4T_1$ (4G)-$^6A_1$ (^6S) transition of Mn^{2+} ions [42], which could be excited by UV light from 200 nm to 300 nm (Fig. 2C). The prepared PLNR gave the quantum yield of 9.4%, and exhibited excellent long persistent luminescence features after excitation with a 254 nm UV lamp for 5 min (Fig. 2D).

PLNR-NH_2 was prepared by anchoring –NH_2 group on the surface of PLNR using APTES via a sol-gel process [34]. The appearance of the strong absorption bands of O–Si–O stretching vibration at 1125 and 1040 cm^{-1}, the asymmetric and symmetric -CH_2- stretching bands at 2933 and 2878 cm^{-1}, and the N–H stretching bands between 3416 and 3248 cm^{-1} in FT-IR spectra confirm the successful amino functionalization of PLNR (Fig. 2E). Subsequent functionalization of PLNR-NH_2 with the thiol modified OTA aptamer was performed to obtain PLNR-Apt through a bifunctional crosslinker sulfo-SMCC. The zeta potential of PLNR-NH_2 in Tris-HCl buffer at pH 8.0 was 10.8 mV, whereas further modification with OTA aptamer caused an opposite shift to −38.5 mV (Fig. 2F), indicating the successful preparation of PLNR-Apt.

AuNP was prepared using a classical citrate reduction method [40,41]. The synthesized AuNP was spherical with an uniform size of 13 ± 2 nm (Fig. 3A) and a strong visible absorption band at approximately 520 nm overlapping greatly with the persistent luminescence emission spectrum of PLNR (Fig. 3B), which enabled the LRET process between PLNR and AuNP. SH-cDNA modification of AuNP gave AuNP-cDNA with an obvious increase in the visible absorption peak

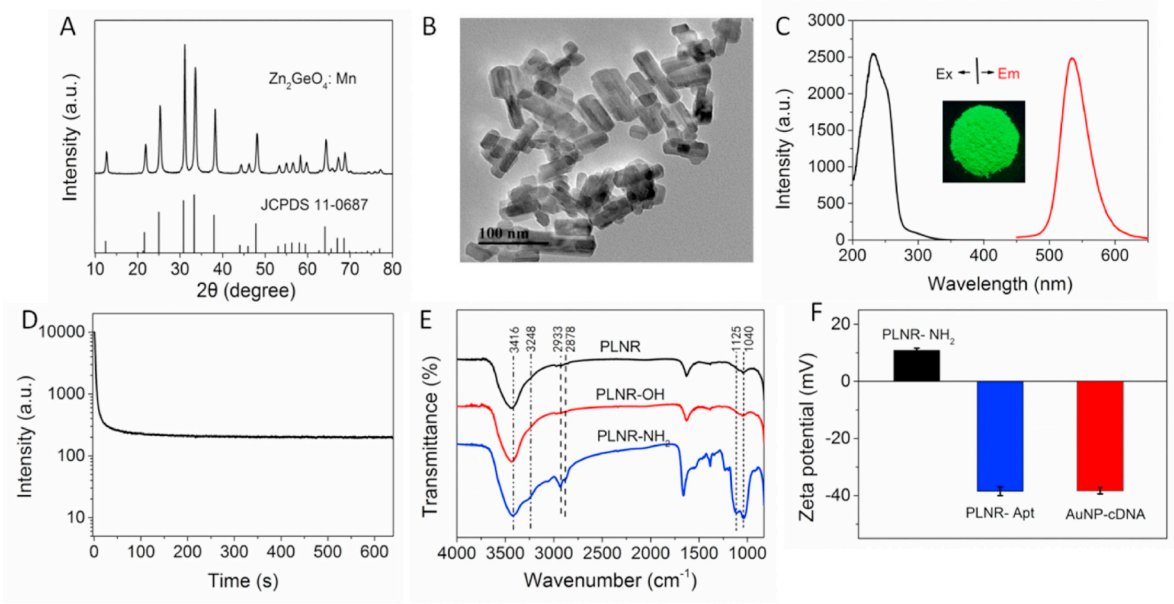

Fig. 2. (A) XRD pattern of the as-prepared PLNR. (B) TEM image of the as-prepared PLNR. (C) Excitation (em. 536 nm) and emission (ex. 254 nm) spectra of the as-prepared PLNR aqueous solution (Excitation: 0.1 mg mL^{-1}; emission: 0.2 mg mL^{-1}). The inset shows photo of the as-prepared PLNR powder under UV excitation. (D) Persistent luminescence decay curve of PLNR monitored at 536 nm after 5-min excitation with a 254 nm UV lamp. (E) FT-IR spectra of PLNR, PLNR-OH and PLNR-NH_2. (F) Zeta potentials of the functionalized nanoparticles in Tris-HCl buffer (pH 8.0).

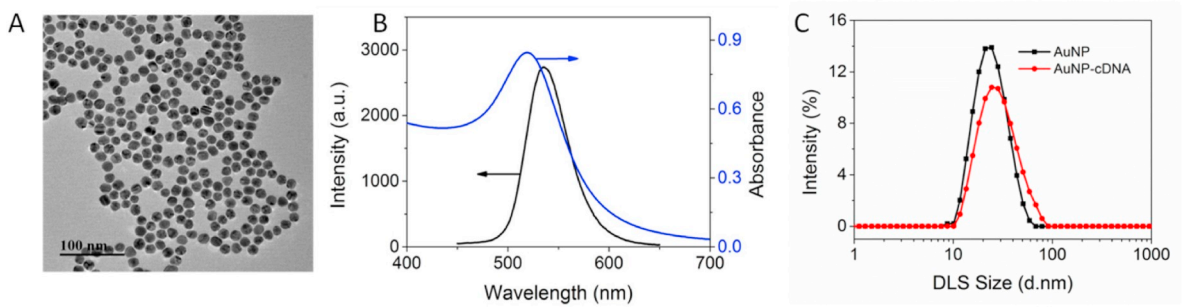

Fig. 3. (A) TEM image of the as-prepared AuNP. (B) Luminescence spectrum of the as-prepared PLNR (0.2 mg mL^{-1}) and the absorption spectrum of the as-prepared AuNP. (C) Hydrodynamic dimeter distribution of the AuNP before and after DNA conjugation.

intensity at 260 nm from the DNA (Fig. S1). Furthermore, AuNP-cDNA had larger hydrodynamic size than the bare AuNP (Fig. 3C), also indicating successful conjugation of AuNP and SH-cDNA. The zeta potential of AuNP-cDNA in Tris-HCl buffer at pH 8.0 was −38.2 mV (Fig. 2F). It should be noted that both PLNR-Apt and AuNP-cDNA were negatively charged, which indicates that the formation of LRET pair was based on DNA hybridization rather than electrostatic interaction.

3.3. Optimization of detection conditions

We first studied the effect of the concentration of AuNP-cDNA and reaction time on the hybridization of AuNP-cDNA and PLNR-Apt. The concentration of AuNP-cDNA was carefully optimized with 0.15 mg mL^{-1} PLNR-Apt. The persistent luminescence intensity of PLNR-Apt decreased gradually as the concentration of AuNP-cDNA increased due to the formation of LRET pair between PLNR-Apt and AuNP-cDNA (Fig. 4A). However, the quenching efficiency reached a plateau over 140 pmol L^{-1} AuNP-cDNA (Fig. 4B). Considering that excessive AuNP-cDNA would lead to nonspecific quenching, thus was unfavorable for subsequent luminescence recovery, a AuNP-cDNA concentration of 120 pmol L^{-1} corresponding to the quenching efficiency of 76.4% was finally selected. The effect of hybridization time on the persistent luminescence intensity of 0.15 mg mL^{-1} PLNR-Apt was studied with 120 pmol L^{-1} AuNP-cDNA. The quenched persistent luminescence intensity increased with hybridization time up to 100 min, then kept unchanged with further increase of hybridization time (Fig. 4C). Thus, 120 min hybridization time was used for further experiments.

We then tested the effect of reaction time on the recovery of the persistent luminescence of 0.15 mg mL^{-1} PLNR-Apt in the presence of 120 pmol L^{-1} AuNP-cDNA after adding 5 ng mL^{-1} OTA. The result shows that 40 min was sufficient to quantitatively recover the persistent luminescence of 0.15 mg mL^{-1} PLNR-Apt (Fig. 4D). So, 60 min was selected to ensure the recovery of the persistent luminescence in further work.

Control experiments were carried out to confirm that the persistent luminescence quenching was caused by the nucleic acid hybridization of PLNR-Apt with AuNP-cDNA (Fig. S2). The presence of AuNP (120 pmol L^{-1}) to PLNR-Apt (0.15 mg mL^{-1}) did not lead to obvious change of the persistent luminescence of PLNR-Apt. In contrast, the persistent luminescence of PLNR-Apt was significantly quenched in the presence of AuNP-cDNA (120 pmol L^{-1}). The results suggest that PLNR-Apt and AuNP-cDNA were closed to each other via strong hybridization between complementary DNA and OTA aptamer, leading to the occurrence of LRET process.

3.4. Analytical performance of the developed LRET aptasensor

The detection of OTA under optimal conditions was performed. The persistent luminescence of PLNR-Apt was maximally quenched by

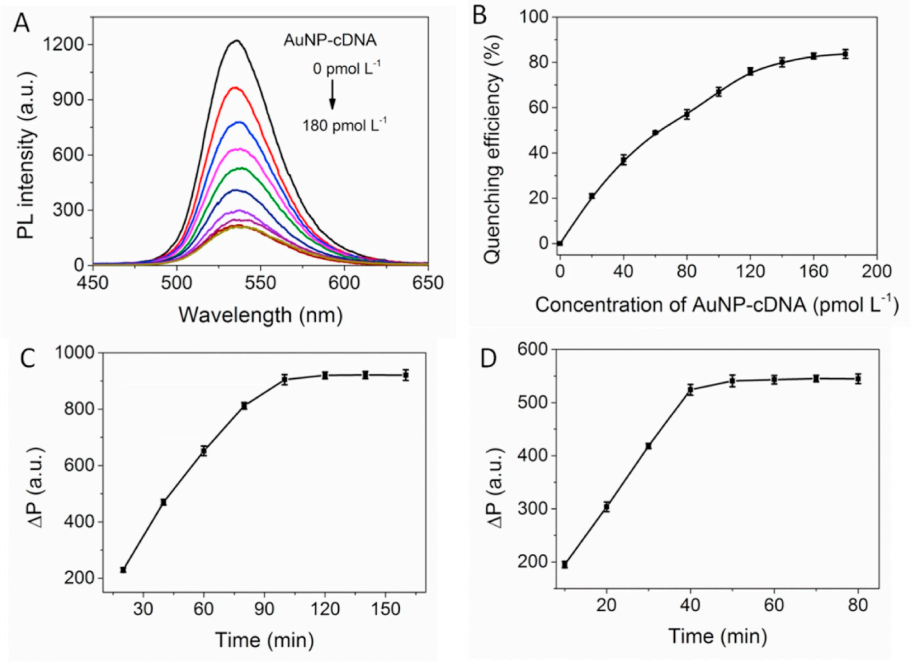

Fig. 4. (A) Effect of AuNP-cDNA concentration on the PL intensity of PLNR-Apt. (B) Change of quenching efficiency with AuNP-cDNA concentration. (C) Time dependence of the quenched luminescence intensity in the presence of 120 pmol L^{-1} AuNP-cDNA. (D) Time dependence of the recovered luminescence intensity. Concentration: PLNR-Apt, 0.15 mg mL^{-1}; AuNP-cDNA, 120 pmol L^{-1}; OTA, 5 ng mL^{-1}.

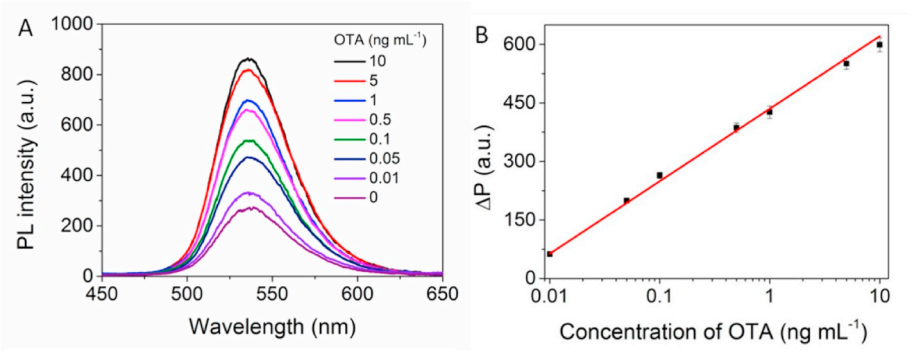

Fig. 5. (A) Recovery of PL intensity in the presence of different concentrations of OTA. (B) Plot of recovered PL intensity versus the concentration of OTA.

AuNP-cDNA in the absence of OTA (Fig. 4A), but recovered in the presence of OTA (Fig. 5A). The recovered luminescence intensity increased with the concentration of OTA (Fig. 5A and B). A good linear relationship between the recovered persistent luminescence intensity (Δp) and the natural logarithm of OTA concentration (C_{OTA}, ng mL^{-1}) was obtained in a range from 0.01 to 10 ng mL^{-1} with a linear regression equation of $\Delta P = 186\log C_{OTA} + 435$ ($R^2 = 0.9974$). The limit of detection (LOD) ($3s$) was calculated to be 3 pg mL^{-1}, which is less than or comparable to those of some reported methods based on nanomaterials for OTA detection (Table S2). The precision for 11 replicate detections of OTA at 1 ng mL^{-1} was 2.7% (relative standard deviation, RSD).

3.5. Specificity of the developed LRET aptasensor

To investigate the specificity of the developed LRET aptasensor for OTA detection, the influence of five other mycotoxins, including ochratoxin B (OTB), fumonisin (FB1), aflatoxin B1 (AFB1), deoxynivalenol (DON) and zearalenone (ZEN) were examined. The concentration of these mycotoxins used was 10 ng mL^{-1}, which is ten times the concentration of OTA. Each type of mycotoxin was added to the prepared detection system individually, and the intensity of the luminescence recovery was recorded after incubation. The results show that only OTA induced a significant persistent luminescence recovery, while none of other mycotoxins caused obvious luminescence changes (Fig. 6), which is attributed to the specific affinity of the aptamer toward OTA. The above results clearly demonstrate that the designed LRET aptasensor has excellent specificity for OTA detection.

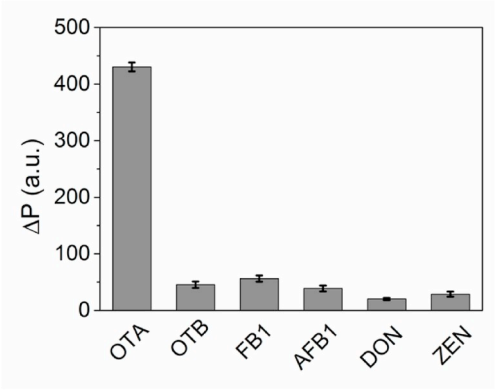

Fig. 6. Luminescence response of the LRET aptasensor to OTA (1 ng mL^{-1}), OTB (10 ng mL^{-1}), FB1 (10 ng mL^{-1}), AFB1(10 ng mL^{-1}), DON(10 ng mL^{-1}) and ZEN (10 ng mL^{-1}).

3.6. Analytical application

To demonstrate the feasibility and applicability of the developed LRET aptasensor, the OTA in beer samples was determined and the recoveries of OTA in the beer samples were measured by spiking the OTA standard solution. Briefly, four kinds of beer samples were spiked with OTA standard solutions in the range of 0.05–0.5 ng mL^{-1}. The results for the determination of OTA in the beer samples by the developed LRET aptasensor are compared with those obtained by the ELISA method (Table 1). The developed LRET aptasensor and the ELISA method gave consistent analytical results. Moreover, the recovery for the spiked OTA ranged from 92.3% to 104%. The results indicate that the applicability of the developed LRET aptasensor for the analysis of real samples.

4. Conclusions

In summary, we have developed a persistent luminescence nanomaterials based LRET aptasensor for the determination of OTA. The developed LRET aptasensor exhibits excellent sensitivity and selectivity because of the long-lasting afterglow feature of PLNR and the high specificity of aptamer toward OTA. Furthermore, the developed LRET aptasensor is capable of detecting OTA in beer samples without autofluorescence interference. This work provides a promising optical sensing strategy for the detection of contaminants in food samples.

Table 1
Analytical results for the determination of OTA in beer samples.

Sample	Spiked OTA (ng mL^{-1})	Concentration determined (Mean ± s, n = 3) (ng mL^{-1})		Recovery (%) (Mean ± s, n = 3)
		Our method	ELISA method	
Beer 1	0	ND	ND	–
	0.05	0.046 ± 0.003	0.052 ± 0.003	92.6 ± 5.1
	0.1	0.095 ± 0.005	0.092 ± 0.004	95.2 ± 4.8
	0.5	0.473 ± 0.018	0.487 ± 0.013	94.7 ± 3.6
Beer 2	0	0.131 ± 0.006	0.139 ± 0.005	–
	0.05	0.177 ± 0.009	0.162 ± 0.007	97.8 ± 4.8
	0.1	0.234 ± 0.006	0.211 ± 0.010	101 ± 3
	0.5	0.602 ± 0.034	0.645 ± 0.017	95.4 ± 5.3
Beer 3	0	ND	ND	–
	0.05	0.046 ± 0.002	0.047 ± 0.002	92.3 ± 4.0
	0.1	0.098 ± 0.007	0.108 ± 0.004	98.1 ± 7.2
	0.5	0.519 ± 0.026	0.490 ± 0.016	104 ± 5
Beer 4	0	ND	ND	–
	0.05	0.048 ± 0.003	0.045 ± 0.002	96.4 ± 6.3
	0.1	0.102 ± 0.008	0.113 ± 0.005	103 ± 7
	0.5	0.481 ± 0.019	0.520 ± 0.021	96.3 ± 3.8

ND: Not detected.

CRediT authorship contribution statement

Yuan-Yuan Jiang: Methodology, Investigation, Data curation, Writing - original draft. **Xu Zhao:** Methodology, Funding acquisition. **Li-Jian Chen:** Methodology, Funding acquisition. **Cheng Yang:** Validation, Data curation. **Xue-Bo Yin:** Supervision. **Xiu-Ping Yan:** Conceptualization, Supervision, Writing - review & editing, Funding acquisition.

Declaration of competing interest

The authors declare no competing financial interest.

Acknowledgments

This work was supported by the National Natural Science Foundation of China (No. 21804056 and 21804057), the China Postdoctoral Science Foundation (No. 2018M630511 and 2018M630509), and the Natural Science Foundation of Jiangsu Province, China (No. BK20180581 and BK20180584), the National First-class Discipline Program of Food Science and Technology (No. JUFSTR20180301), the Fundamental Research Funds for the Central Universities (No. JUSRP51714B and JUSRP11846), and the Program of "Collaborative Innovation Center of Food Safety and Quality Control in Jiangsu Province".

Appendix A. Supplementary data

Supplementary data to this article can be found online at https://doi.org/10.1016/j.talanta.2020.121101.

References

[1] M.L. Fernández-Cruz, M.L. Mansilla, J.L. Tadeo, Mycotoxins in fruits and their processed products: analysis, occurrence and health implications, J. Adv. Res. 1 (2010) 113–122.
[2] Y. Alhamoud, D. Yang, S.S. Fiati Kenston, G. Liu, L. Liu, H. Zhou, F. Ahmed, J. Zhao, Advances in biosensors for the detection of ochratoxin A: bio-receptors, nanomaterials, and their applications, Biosens. Bioelectron. 141 (2019) 111418.
[3] X. Wu, J. Hu, B. Zhu, L. Lu, X. Huang, D. Pang, Advances in biosensors for the detection of ochratoxin A: bio-receptors, nanomaterials, and their applications, J. Chromatogr. A 1218 (2011) 7341–7346.
[4] S. Marin, A.J. Ramos, G. Cano-Sancho, V. Sanchis, Mycotoxins: occurrence, toxicology, and exposure assessment, Food Chem. Toxicol. 60 (2010) 218–237.
[5] A. El Khoury, A. Atoui, Ochratoxin A: general overview and actual molecular status, Toxins 2 (2010) 461–493.
[6] A. Pfohl-Leszkowicz, R.A. Manderville, Ochratoxin A: an overview on toxicity and carcinogenicity in animals and humans, Mol. Nutr. Food Res. 51 (2007) 61–99.
[7] H. Badie Bostan, N.M. Danesh, G. Karimi, M. Ramezani, S.A. Mousavi Shaegh, K. Youssefi, F. Charbgoo, K. Abnous, S.M. Taghdisi, Ultrasensitive detection of ochratoxin A using aptasensors, Biosens. Bioelectron. 98 (2017) 168–179.
[8] L. Covarelli, G. Beccari, A. Marini, L. Tosi, A review on the occurrence and control of ochratoxigenic fungal species and ochratoxin A in dehydrated grapes, non-fortified dessert wines and dried vine fruit in the Mediterranean area, Food Contr. 26 (2012) 347–356.
[9] R. Yamamoto, M. Sawada, N. Yamato, A. Yamamoto, S. Kodama, High-performance liquid chromatography with fluorescence detection of ochratoxin A in cereal, coffee, and wine: effective pretreatment with bovine serum albumin-immobilized adsorbent, Sep. Sci. Plus 1 (2018) 196–201.
[10] M.A. Andrade, F.M. Lancas, Determination of Ochratoxin A in wine by packed in-tube solid phasemicroextraction followed by high performance liquidchromatography coupled to tandem mass spectrometry, J. Chromatogr. A 1493 (2010) 41–48.
[11] G.J. Soleas, J. Yan, D.M. Goldberg, Assay of ochratoxin A in wine and beer by high-pressure liquid chromatography photodiode array and gas chromatography mass selective detection, J. Agric. Food Chem. 49 (2001) 2733–2740.
[12] A. Zhang, Y. Ma, L. Feng, Y. Wang, C. He, X. Wang, H. Zhang, Development of a sensitive competitive indirect ELISA method for determination of ochratoxin A levels in cereals originating from Nanjing, China, Food Contr. 22 (2011) 1723–1728.
[13] N. Kaur, A. Bharti, S. Batra, S. Rana, S. Rana, A. Bhalla, N. Prabhakar, An electrochemical aptasensor based on graphene doped chitosan nanocomposites for determination of Ochratoxin A, Microchem. J. 144 (2019) 102–109.
[14] Z. Sun, Z. Duan, X. Liu, X. Deng, Z. Tang, Development of a nanobody-based competitive dot ELISA for visual screening of ochratoxin A in cereals, Food Anal. Methods 10 (2017) 3558–3564.
[15] I.K. Cigić, H. Prosen, An overview of conventional and emerging analytical methods for the determination of mycotoxins, Int. J. Mol. Sci. 10 (2009) 62–115.
[16] L. Sheng, J. Ren, Y. Miao, J. Wang, E. Wang, PVP-coated graphene oxide for selective determination of ochratoxin A via quenching fluorescence of free aptamer, Biosens. Bioelectron. 26 (2011) 3494–3499.
[17] Z. Lu, X. Chen, W. Hu, A fluorescence aptasensor based on semiconductor quantum dots and MoS_2 nanosheets for ochratoxin A detection, Sens. Actuators, B 246 (2017) 61–67.
[18] E.J. Jo, J.Y. Byun, H. Mun, D. Bang, J.H. Son, J.Y. Lee, L.P. Lee, M.G. Kim, Single-Step LRET aptasensor for rapid mycotoxin detection, Anal. Chem. 90 (2018) 716–722.
[19] S. Dai, S. Wu, N. Duan, J. Chen, Z. Zheng, Z. Wang, An ultrasensitive aptasensor for Ochratoxin A using hexagonal core/shell upconversion nanoparticles as luminophores, Biosens. Bioelectron. 26 (2017) 538–544.
[20] J. Wang, Q. Ma, Y. Wang, H. Shen, Q. Yuan, Recent progress in biomedical applications of persistent luminescence nanoparticles, Nanoscale 9 (2017) 6204–6218.
[21] Y. Li, M. Gecevicius, J. Qiu, Long persistent phosphors—from fundamentals to applications, Chem. Soc. Rev. 45 (2016) 2090–2136.
[22] K. Van den Eeckhout, P.F. Smet, D. Poelman, Persistent luminescence in non-Eu^{2+}-doped compounds: a review, Materials 3 (2010) 2536–2566.
[23] Z. Pan, Y.-Y. Lu, F. Liu, Sunlight-activated long-persistent luminescence in the near-infrared from Cr^{3+}-doped zinc gallogermanates, Nat. Mater. 11 (2012) 58–63.
[24] Q.L.M. de Chermont, C. Chaneac, J. Seguin, F. Pelle, S. Maitrejean, J.P. Jolivet, D. Gourier, M. Bessodes, D. Scherman, Nanoprobes with near-infrared persistent luminescence for in vivo imaging, Proc. Natl. Acad. Sci. U. S. A 104 (2007) 9266–9271.
[25] T. Maldiney, B. Viana, A. Bessière, D. Gourier, M. Bessodes, D. Scherman, C. Richard, In vivo imaging with persistent luminescence silicate-based nanoparticles, Opt. Mater. 35 (2013) 1852–1858.
[26] T. Maldiney, A. Bessière, J. Seguin, E. Teston, S.K. Sharma, B. Viana, A.J. Bos, P. Dorenbos, M. Bessodes, D. Gourier, D. Scherman, C. Ricard, The in vivo activation of persistent nanophosphors for optical imaging of vascularization, tumours and grafted cells, Nat. Mater. 13 (2014) 418–426.
[27] B.-Y. Wu, H.-F. Wang, J.-T. Chen, X.-P. Yan, Fluorescence resonance energy transfer inhibition assay for r-fetoprotein excreted during cancer cell growth using functionalized persistent luminescence nanoparticles, J. Am. Chem. Soc. 133 (2011) 686–688.
[28] N. Li, Y. Li, Y. Han, W. Pan, T. Zhang, B. Tang, A highly selective and instantaneous nanoprobe for detection and imaging of ascorbic acid in living cells and in vivo, Anal. Chem. 86 (2014) 3924–3930.
[29] B.-Y. Wu, X.-P. Yan, Bioconjugated persistent luminescence nanoparticles for Főster resonance energy transfer immunoassay of prostate specific antigen in serum and cell extracts without in situ excitation, Chem. Commun. 51 (2015) 3903–3906.
[30] J. Shi, X. Sun, J. Zhu, J. Li, H. Zhang, One-step synthesis of amino-functionalized ultrasmall near infrared-emitting persistent luminescent nanoparticles for in vitro and in vivo bioimaging, Nanoscale 8 (2016) 9798–9804.
[31] J. Wang, Q. Ma, X. Hu, H. Liu, W. Zheng, X. Chen, Q. Yuan, W. Tan, Autofluorescence-free targeted tumor imaging based on luminous nanoparticles with composition-dependent size and persistent luminescence, ACS Nano 11 (2017) 8010–8017.
[32] Y.-J. Li, X.-P. Yan, Synthesis of functionalized triple-doped zinc gallogermanate nanoparticles with superlong near-infrared persistent luminescence for long-term orally administrated bioimaging, Nanoscale 8 (2016) 14965–14970.
[33] S.-Q. Wu, C.-W. Chi, C.-X. Yang, X.-P. Yan, Penetrating peptide-bioconjugated persistent nanophosphors for long-term tracking of adipose-derived stem cells with superior signal-to-noise ratio, Anal. Chem. 88 (2016) 4114–4121.
[34] A. Abdukayum, J.-T. Chen, Q. Zhao, X.-P. Yan, Functional near infrared-emitting Cr^{3+}/Pr^{3+} Co-doped zinc gallogermanate persistent luminescent nanoparticles with superlong afterglow for in vivo targeted bioimaging, J. Am. Chem. Soc. 135 (2013) 14125–14133.
[35] J. Shi, X. Sun, J. Li, H. Man, J. Shen, Y. Yu, H. Zhang, Multifunctional near infrared-emitting long-persistence luminescent nanoprobes for drug delivery and targeted tumor imaging, Biomaterials 37 (2015) 260–270.
[36] B. Zheng, H. Chen, P. Zhao, H. Pan, X. Wu, X. Gong, H. Wang, J. Chang, Persistent luminescent nanocarrier as an accurate tracker in vivo for near infrared-remote selectively triggered photothermal therapy, ACS Appl. Mater. Interfaces 8 (2016) 21603–21611.
[37] R. Abdurahman, C.-X. Yang, X.-P. Yan, Conjugation of a photosensitizer to near infrared light renewable persistent luminescence nanoparticles for photodynamic therapy, Chem. Commun. 52 (2016) 13303–13306.
[38] J. Wang, Q. Ma, W. Zheng, H. Liu, C. Yin, F. Wang, X. Chen, Q. Yuan, W. Tan, One-dimensional luminous nanorods featuring tunable persistent luminescence for autofluorescence-free biosensing, ACS Nano 11 (2017) 8185–8191.
[39] J. Wang, Q. Ma, H. Liu, Y. Wang, H. Shen, X. Hu, C. Ma, Q. Yuan, W. Tan, Time-gated imaging of latent fingerprints and specific visualization of protein secretions via molecular recognition, Anal. Chem. 89 (2017) 12764–12770.
[40] K.C. Grabar, R.G. Freeman, M.B. Hommer, M.J. Natan, Preparation and characterization of Au colloid monolayers, Anal. Chem. 67 (1995) 735–743.
[41] Y. Wu, J. Huang, X. Yang, Y. Yang, K. Quan, N. Xie, J. Li, C. Ma, K. Wang, Gold nanoparticle loaded split-DNAzyme probe for amplified miRNA detection in living cells, Anal. Chem. 89 (2017) 8377–8383.
[42] Y.-H. Lee, L.-Y. Luo, N.-S. Wang, T.-M. Chen, Luminescence and time-resolved fluorescence decay of Mn^{2+} -activated Zn_2GeO_4 phosphors under ultraviolet excitation, Chin. J. Lumin. 26 (2005) 183–188.